Physicochem. Probl. Miner. Process., 62(3), 2026, 224462

http://www.journalssystem.com/ppmp

Physicochemical Problems of Mineral Processing

ISSN 1643-1049

Mechanistic insights into the selective flotation separation of brucite from quartz using octadecyl trimethyl ammonium chloride surfactant

Weijun Tan [1], Guoxian Huang [2], Nan Zhang [1], Yanqing Gong [1], Fei Li [2], Zhongyuan Zhao [2], Yingcai Chen [2]

[1] Qinghai Jinchuan Mining Co., Ltd., Haidong 810700, China

[2] Northwest Institute of Mining and Metallurgy, Baiyin 730900, China

Corresponding author: sun18530788241@163.com (Guoxian Huang)

Abstract: The development of efficient collectors is key to achieving the flotation separation of brucite and quartz. This study systematically investigated the separation performance and mechanism of action of the cationic surfactant octadecyl trimethyl ammonium chloride (STAC) as a novel collector for brucite and quartz. Under conditions of 30 mg/L STAC concentration, pH 7.0, and a flotation cell agitation speed of 2000 rpm, efficient separation of the two minerals was successfully achieved. Contact angle and zeta potential measurements indicate that STAC exhibits significant selectivity toward brucite and quartz. After STAC treatment, the changes in the contact angle and zeta potential of quartz were 7.82 and 57.1 times those of brucite, respectively, indicating that STAC selectively adsorbed onto the quartz surface while exerting only a weak effect on brucite. Fourier Transform Infrared Spectroscopy (FTIR) and X-ray Photoelectron Spectroscopy (XPS) analysis further revealed that the positively charged quaternary ammonium head groups in the STAC molecules preferentially bind to oxygen atoms on the quartz surface, with a binding energy change 3.2 times greater than that observed for brucite. These results confirm that STAC selectively acts on the quartz surface via an electrostatic adsorption mechanism, while exhibiting only negligible adsorption on brucite, thereby achieving efficient flotation separation of the two minerals.

Keywords: brucite, quartz, STAC, flotation, selective adsorption

1. Introduction

As an important inorganic layered mineral resource, brucite ($Mg(OH)_2$) has become a hot topic of research in the global fields of new materials and environmental remediation due to its high magnesium content (theoretical MgO content as high as 69%), excellent thermal stability, and environmentally friendly properties (Zhu et al., 2026; Fu et al., 2023; Sun et al., 2025). China possesses superior brucite resources with abundant reserves. Among these, the high-quality fibrous deposits from the Kuandian region of Liaoning Province are particularly notable, with a purity approaching the theoretical value, providing a solid raw material foundation for the development of high-value-added magnesium-based products (Gong et al., 2023; Liu et al., 2025). In terms of traditional industrial applications, brucite, with its natural alkalinity and adsorption properties, has demonstrated significant advantages in the pharmaceutical sector as an antacid, in agriculture as a soil conditioner and magnesium fertiliser, and in environmental protection for the treatment of acidic wastewater and the removal of heavy metals (Gong et al., 2024; Yin et al., 2025). In recent years, with the deepening advancement of green and environmentally friendly concepts, research on magnesium hydroxide-based carbon dioxide capture and flue gas desulfurization technologies has achieved continuous breakthroughs, further highlighting its strategic importance in comprehensive resource utilisation and the circular economy.

However, with the rapid development of the magnesium chemical industry, high-grade brucite concentrate resources are becoming increasingly scarce, making it inevitable to shift the focus of development and utilisation toward low-grade ores. Natural brucite is often associated with quartz (SiO_2), and both minerals exhibit strong hydrophilic properties. Conventional gravity or magnetic

DOI: 10.37190/ppmp/224462

separation methods struggle to achieve effective separation; therefore, flotation must be employed, utilising selective collectors to modulate the physicochemical properties of the mineral surfaces. However, traditional amine collectors, such as dodecylamine, exhibit strong foaming properties (Ao et al., 2026; Zhang et al., 2024; Liu et al., 2024). Due to electrostatic interactions, they tend to adsorb onto both brucite and quartz surfaces, resulting in poor separation selectivity and flotation performance that fails to meet industrial requirements. Consequently, the development of novel reagents that combine high selectivity with efficient collection capacity has become a key scientific challenge in enhancing the comprehensive utilisation of brucite resources.

Surfactant octadecyl trimethyl ammonium chloride (STAC) is a typical quaternary ammonium cationic surfactant. Its molecular structure features an octadecyl (C18) chain as the hydrophobic backbone, with three methyl groups attached to the quaternary ammonium nitrogen atom, resulting in a unique amphiphilic structure characterised by a "long hydrophobic tail and a hydrophilic quaternary ammonium head." The molecular structure of STAC is shown in Fig.1. This structure endows STAC with excellent surface activity, good water solubility, and stable cationic characteristics. In desilication processes, conventional amine collectors, such as dodecylamine, hexadecylamine, and octadecylamine, have been widely used to separate silicate minerals from valuable minerals. However, these agents often suffer from limited selectivity when used alone, strict temperature requirements, and flotation performance that is strongly affected by pulp conditions. Based on previous studies, quaternary ammonium collector agents such as ODD and DTAC have demonstrated significant advantages in the flotation separation of silicate and carbonate minerals. However, STAC possesses a longer hydrocarbon chain and stronger hydrophobicity than several commonly used short-chain quaternary ammonium collectors, which may enhance its collecting ability toward quartz. Consequently, STAC holds promising prospects for the flotation separation of brucite and quartz (Yao et al., 2025; Sun et al., 2024). Therefore, using STAC as a collector for the separation of brucite and quartz offers considerable potential and may broaden its application prospects in mineral processing. In daily life, STAC is commonly used in personal care products such as fabric softeners and hair conditioners, where it adsorbs onto the surfaces of fibres or hair strands to provide antistatic and softening effects (Li et al., 2026). In the industrial sector, STAC is widely used as a phase-transfer catalyst, biocide, bitumen emulsifier, and oil recovery aid in oilfields (Li et al., 2025; Sun et al., 2025; Zhang et al., 2021). Given STAC's molecular characteristics—combining a long-chain hydrophobic backbone with a cationic quaternary ammonium head group—it is expected to preferentially adsorb onto negatively charged quartz surfaces through electrostatic attraction, while showing only weak adsorption on positively charged brucite under neutral conditions. Therefore, this study aims to utilise STAC as a novel collector for the flotation separation of brucite and quartz, systematically investigating its flotation behaviour and mechanism of action, with the goal of providing new technical pathways and theoretical support for the efficient and clean utilisation of low-grade brucite resources.

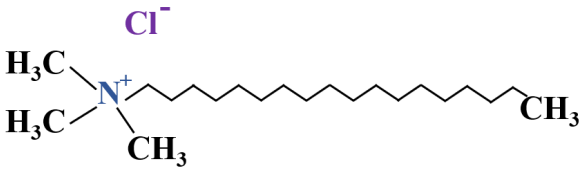

Fig. 1. Molecular structure of STAC

In this study, we first evaluated the effect of STAC on the separation of brucite and quartz through flotation experiments. Subsequently, we employed various characterisation techniques, including contact angle measurements, zeta potential analysis, Fourier-transform infrared spectroscopy (FTIR), and X-ray photoelectron spectroscopy (XPS), to investigate the interaction mechanisms between STAC and mineral surfaces in depth. This study aims to evaluate STAC as a selective collector for the reverse flotation separation of brucite from quartz, thereby effectively addressing the challenges posed by the dwindling supply of high-grade brucite resources and the difficulty in separating brucite due to gangue contamination. Furthermore, it proposes a novel chemical treatment scheme and elucidates its underlying mechanisms, which can guide the design of efficient desilification processes.

2. Materials and methods

2.1. Materials and reagents

The brucite sample used in this study was collected from Kuandian, Liaoning Province, while the quartz sample was obtained from Huangshi, Hubei Province. Prior to experimentation, the raw ores were subjected to pretreatment, including crushing and vibratory sieving, to obtain mineral fractions with a particle size range of -75 to +44 μm. The powders were then thoroughly homogenised for subsequent tests. The mineralogical compositions of the samples were confirmed by X-ray diffraction (XRD) analysis, with the resulting patterns shown in Fig. 2. The results of the multi-element chemical analysis are presented in Table 1. The purities of quartz and brucite were determined to be 99.13% and 99.34%, respectively, which fully satisfy the rigorous requirements for single-mineral flotation experiments. The STAC reagent used in this study was of analytical grade and purchased from Shanghai Aladdin Biochemical Technology Co., Ltd. The pH of the slurry was adjusted using sodium hydroxide (NaOH) or hydrochloric acid (HCl). All chemical reagents were of analytical grade and were diluted to the desired concentrations with deionised water prior to use.

Table 1. The chemical composition of mineral samples

Sample	MgO	Al_2O_3	CaO	SiO_2	TFe	Purity
Brucite	68.66	0.22	0.11	0.57	0.16	99.34
Quartz	-	-	-	99.13	0.13	99.13

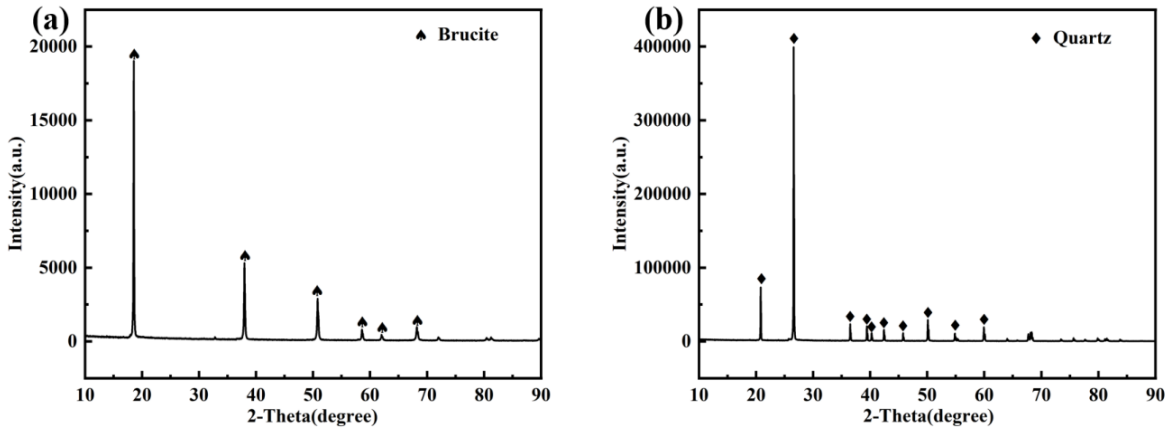

Fig. 2. The XRD analysis of mineral samples

2.2. Experimental methods

In flotation experiments involving single-mineral and binary mixed ores of brucite and quartz, a 2 g sample of ore was used in each experiment. The experiments were conducted using a hanging tank flotation machine with a 30 cm^3 cell capacity. Initially, the slurry was agitated for 2 minutes, after which the pH was adjusted and the collector was added following the sequence specified in the flotation procedure. The froth scraping process lasted 3 minutes, with the flotation machine operating at a rotational speed of 2000 rpm. It should be noted that no additional foaming agent was added during the experiment, as STAC itself provided sufficient foaming capacity under the experimental conditions. Additionally, 20 cm^3 of deionized water was introduced during the test. After flotation, each concentrate was dried and weighed. The flotation experiment procedure is illustrated in Fig. 3. All flotation experiments were repeated three times under identical conditions. The data points in Figs. 4–6 represent averages, and the error bars indicate one standard deviation.

In each experiment, the concentrate was dried to a constant weight and subsequently weighed. The mineral recovery (ε, %) was determined using Equation (1), where the variables are defined as follows: ε represents the mineral recovery (%); β is the grade of the target mineral (expressed as MgO or SiO_2) in the concentrate (%); θ denotes the grade of the target mineral (MgO or SiO_2) in the tailings (%); mc is the mass of the concentrate (g); and mt is the mass of the tailings (g).

$$\varepsilon = \frac{\beta m_c}{\beta m_c + \theta m_t} \times 100\% \quad (1)$$

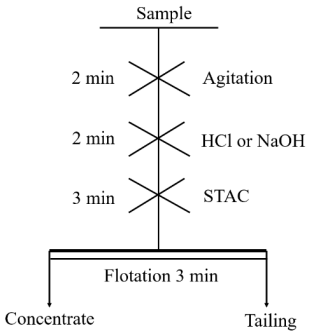

Fig. 3. Floating process flow chart

2.3. Contact angle measurements

The surface wettability of minerals was determined using a Krüss DSA25 drop shape analyzer (Germany). In each test, the ore sample was first stirred with deionized water for 2 min to ensure uniform dispersion, followed by pH adjustment to 7.0 and conditioning with 30 mg/L STAC for 3 min. The solid residue was then filtered and rinsed three times with distilled water. The dried sample was compressed into cylindrical pellets (1.0 cm in diameter × 0.2 cm in thickness) using an electric tablet press under a pressure of 490,000 N. Wettability was evaluated by depositing a water droplet (approximately 3 mm in diameter) onto the polished pellet surface and measuring the contact angle.

2.4. Zeta potential test

The zeta potential of brucite and quartz particles was measured using a Brookhaven NanoBrook Omni instrument (USA) to evaluate the effect of STAC on the surface electrical properties of the minerals. Prior to measurement, the mineral samples were dispersed ultrasonically to prevent particle aggregation. Suspensions were prepared at a solid-to-liquid ratio of 1:100, and the pulp pH was adjusted to the desired values using HCl or NaOH. The zeta potentials of brucite and quartz were measured as a function of pH before and after treatment with 30 mg/L STAC, with at least three replicate measurements performed under each condition and the average values reported. The influence of STAC on surface charge modification was investigated using electrophoretic light scattering (ELS) technique.

2.5. FTIR analysis

FT-IR spectroscopy was conducted using a Nicolet iS20 spectrometer to characterize brucite and quartz surfaces before and after STAC treatment, over a wavenumber range of 400–4000 cm^{-1}. Samples were prepared using the KBr pellet technique. In each preparation, 2 g of mineral sample was mixed with 50 cm^3 of deionized water, and 30 mg/L of STAC was added under pH 7.0 conditions. The suspension was centrifuged at 500 rpm for 20 min, and the solid residue was vacuum-dried. The dried sample was then mixed with KBr, ground, and pressed into pellets for FT-IR analysis.

2.6. XPS analysis

XPS analysis was conducted using a Thermo Scientific K-Alpha spectrometer to characterize brucite and quartz surfaces before and after STAC treatment at pH 7.0. For each sample preparation, 2 g of mineral was dispersed in 20 cm^3 of deionized water, followed by addition of 30 mg/L STAC. The suspension was centrifuged at 500 rpm for 20 min. The solid residue was then dried and subjected to XPS analysis.

3. Experimental results

3.1. Single mineral floatability experiment

3.1.1. Influence of STAC concentration on mineral floatability

The flotation response of brucite and quartz as a function of STAC concentration was evaluated under fixed conditions of pH 7.0 and a stirring speed of 2000 rpm. The resulting data are illustrated in Fig. 4.

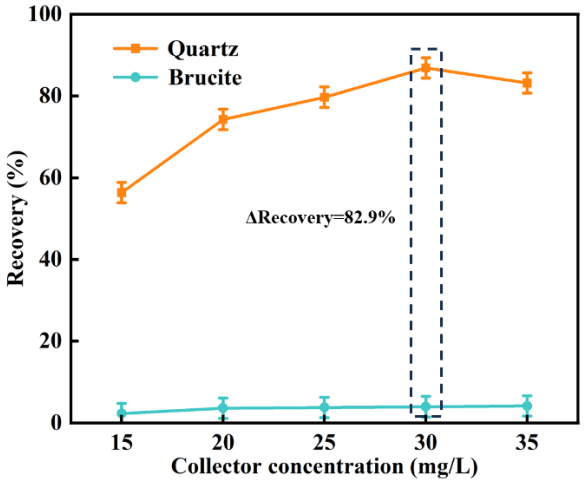

Fig. 4. Influence of STAC concentration on the floatability of brucite and quartz

As shown in Fig. 4, the effect of STAC concentration on the froth flotation behaviour of brucite and quartz was investigated. At a concentration of 15 mg/L, the recovery of quartz reached 56.34%, whereas that of brucite was only 2.31%. When the concentration was increased to 30 mg/L, the quartz recovery reached 86.87%, while the brucite recovery remained low at 3.97%. Further increasing the concentration to 35 mg/L resulted in a slight decrease in quartz recovery, with brucite recovery still below 5%. At the optimal concentration of 30 mg/L, the recovery difference between quartz and brucite reached 82.90%, indicating excellent selectivity of STAC for quartz flotation. Consequently, 30 mg/L of STAC was identified as the optimal concentration.

3.1.2. Influence of pH on mineral floatability

The effect of pulp pH on the flotation behaviour of brucite and quartz was investigated at a fixed STAC concentration of 30 mg/L and a stirring speed of 2000 rpm.The results are presented in Fig. 5.

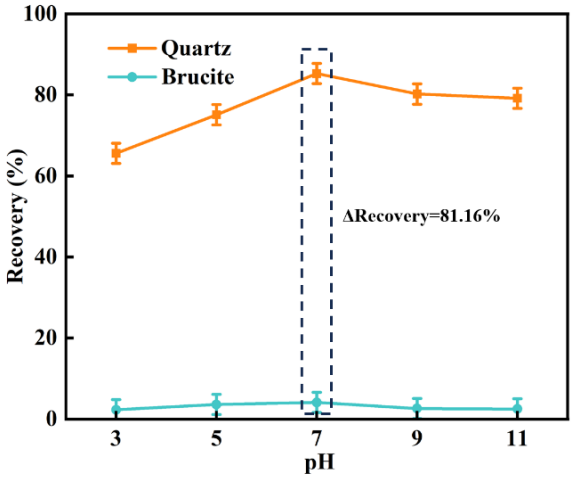

Fig. 5. Influence of pH on the floatability of brucite and quartz

The results in Fig. 5 indicated that pH has a significant effect on the flotation behaviour of brucite and quartz. The recovery of quartz initially increased and then decreased as the pH rose, peaking at 85.26% at pH 7.0. Subsequently, as the pH increased to 11.0, the recovery gradually decreased to 79.16%. In contrast, the recovery of brucite remained below 5% across the entire tested pH range (3.0–11.0) and was minimally affected by pH. Overall, the difference in recovery between the two minerals was greatest at pH 7.0, with a recovery of 81.16%. Therefore, pH 7.0 was determined to be the optimal condition for achieving selective separation of the two minerals.

3.1.3. Influence of flotation cell speed on mineral floatability

With the pulp pH maintained at 7.0 and the STAC concentration held constant at 30 mg/L, flotation experiments were conducted to examine the influence of stirring speed on the flotation behaviour of brucite and quartz, as shown in Fig. 6.

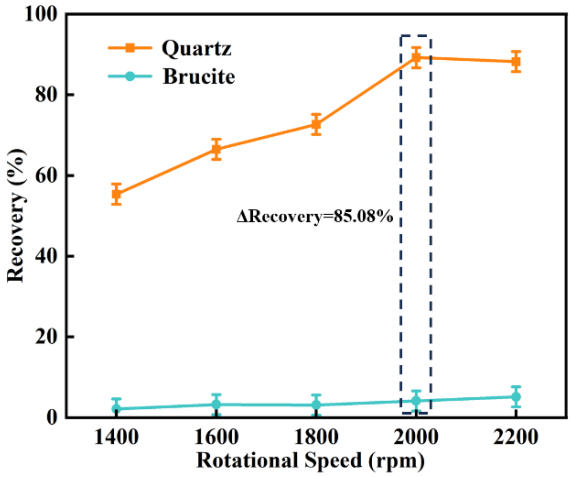

Fig. 6. The influence of flotation cell speed on the floatability of brucite and quartz

Fig. 6 illustrates the effect of flotation cell rotation speed on mineral floatability. When the rotation speed was increased from 1400 r/min to 2000 r/min, the quartz recovery rose significantly from 55.36% to a maximum of 89.21%; thereafter, when the rotation speed was further increased to 2200 r/min, quartz recovery plateaued and slightly decreased, which can be attributed to excessive hydrodynamic turbulence. Although higher speeds increase the frequency of bubble-particle collisions, they also increase the shear forces acting on the attached particles, promoting their desorption from the bubble surface and ultimately limiting further improvement in flotation recovery. At the optimal rotational speed of 2000 r/min, the difference in recovery between the two reached a maximum of 85.08%, achieving highly efficient separation.

3.2. Artificial mixed ore flotation separation experiment

To further investigate the flotation separation of brucite under various conditions, flotation experiments were conducted using artificially mixed ores, following the experimental procedure shown in Fig. 3. Table 2 presents the results of these experiments, which utilised a total of 2.0 g of ore, with the brucite-to-quartz ratio set at 1:1 and 7:3, respectively. It should be noted that the concentrate in the mixed ore test refers to the product in the cell (brucite), not the froth product (quartz). STAC selectively hydrophobizes quartz, causing it to enter the froth and be discarded as tailings, while hydrophilic brucite remains in the cell and is collected as the final concentrate. This reverse flotation configuration explains why the concentrate exhibits high MgO grades and low quartz recovery, which is fully consistent with the results of single-mineral flotation.

Based on the data in Table 2, for mixed ores with brucite-to-quartz mass ratios of 1:1 and 7:3, quartz recovery in the concentrate remained consistently below 10% with low SiO_2 content (1.23–1.57%), while

Table 2. Artificial mixed ore experiment results

Mixed ore ratio	Sample	Productivity/%	Grade /%		Recovery /%	
			MgO	SiO_2	Brucite	Quartz
Brucite:	concentrate	46.42	66.62	1.57	89.69	3.41
Quartz =1:1	ore	100.00	34.27	50.00	100.00	100.00
Brucite:	concentrate	65.97	67.67	1.23	92.48	4.13
Quartz =7:3	ore	100.00	47.84	5.08	100.00	100.00

brucite recovery reached 89.69–92.48% and MgO grade stabilized at 66.62–67.67%, confirming that STAC exhibits excellent selective separation performance regardless of ore ratio. It is noteworthy that mechanical entrainment of fine quartz particles is a common issue in brucite flotation; however, the strong and selective hydrophobization of quartz by STAC (contact angle increased from 15.27° to 58.69°) promotes bubble attachment and selective flotation of quartz, which may help reduce the transfer of quartz into the concentrate. Thus, STAC enables selective separation and provides solid experimental support for the preparation of high-purity brucite concentrate from natural low-grade ores.

3.3. Mechanism of action analysis

3.3.1. Contact angle measurements results

The contact angle is an important parameter for characterising the wettability of mineral surfaces; it directly reflects the degree of hydrophobicity of the minerals and, consequently, determines their flotation response (Sun et al., 2026; Kruszelnicki et al., 2024). Generally speaking, the larger the contact angle, the more pronounced the hydrophobicity of the mineral surface, and the easier it is for the mineral to adhere to bubbles and float to the surface (Ma et al., 2023; Yao et al., 2024).Fig. 7 presents a comparison of the contact angles of the two minerals before and after treatment with 30 mg/L STAC.

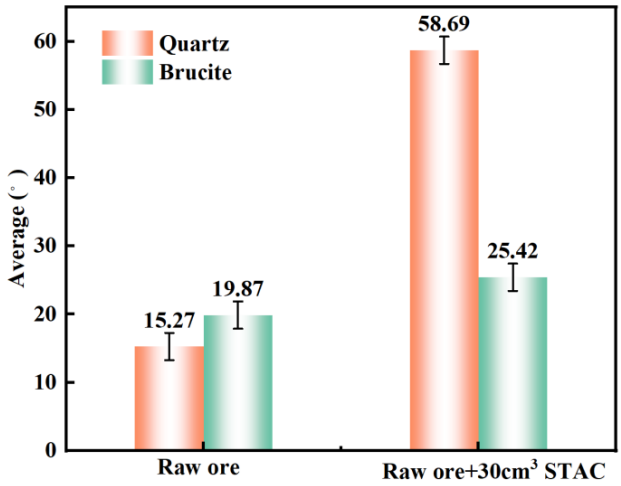

Fig. 7. Comparison of contact angle changes of minerals before and after treatment with 30 mg/L STAC

Fig. 7 shows the changes in the contact angles of the minerals before and after STAC treatment. Without chemical treatment, the initial contact angles of quartz and brucite were approximately 15.27° and 19.87°, respectively, with both exhibiting strong hydrophilicity. After treatment with 30 mg/L STAC, the contact angle of quartz increased significantly to 58.69°, indicating a transformation from a hydrophilic to a hydrophobic surface. In contrast, the contact angle of brucite changed only slightly. Calculations show that the difference in contact angles between the two reached 33.27°, and the change in the contact angle of quartz was approximately 7.82 times that of brucite. This result indicates that STAC selectively adsorbs onto the quartz surface rather than the brucite surface, thereby significantly enhancing the hydrophobic properties of quartz.

3.3.2. Zeta potential results

During the flotation process, reagents alter the interfacial properties of minerals by adsorbing onto their surfaces, ultimately affecting the minerals' floatability (Zhao et al., 2022; Sun et al., 2025). To gain a deeper understanding of the interaction mechanism between reagents and minerals, zeta potential measurements are commonly employed to characterise the changes in mineral surface charge under different pH conditions (Hu et al., 2026). Fig. 8 presents the zeta potential measurement results for brucite and quartz as a function of pH, both before and after STAC treatment.

As shown in Fig. 8, the isoelectric points of natural quartz and brucite were approximately pH 2.1 and pH 10.0, respectively, which are generally consistent with values reported in the literature (Liu et al., 2025;

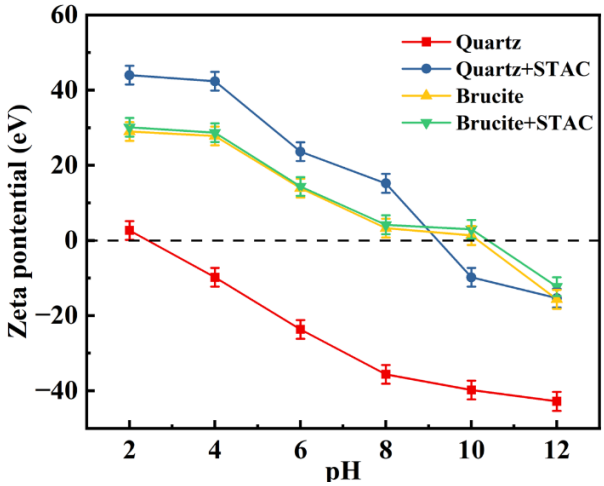

Fig. 8. Changes in zeta potential on mineral surfaces under different pH conditions

Ban et al., 2025). Across the acidic to alkaline pH range, the zeta potential of quartz exhibited a substantial positive shift after STAC treatment, with changes ranging from 24.2 to 49.6 mV. In contrast, the variation in the zeta potential of brucite was negligible, never exceeding 2.0 mV over the entire pH range investigated. Under the optimal pH condition (7.0) determined by single-mineral flotation experiments, STAC exhibited the most pronounced selective adsorption on quartz. At this pH, the quartz surface carried a strong negative charge, with a zeta potential of −35.63 mV. Upon STAC treatment, its zeta potential shifted sharply in the positive direction to +15.19 mV, corresponding to a substantial change of 50.82 mV. By contrast, brucite exhibited a weak positive surface charge at pH 7.0, with a zeta potential of +3.28 mV, which increased only marginally to +4.17 mV after STAC treatment—a change of merely 0.89 mV. The magnitude of the zeta potential shift for quartz was approximately 57.1 times that of brucite. Under the optimum flotation condition (pH 7.0), quartz carried a strong negative charge (−35.63 mV), whereas brucite remained weakly positive (+3.28 mV). These results demonstrate that the positively charged STAC cations preferentially adsorb onto the negatively charged quartz surface via electrostatic attraction, while only weak adsorption occurs on the weakly positive brucite surface, providing direct electrostatic evidence for the adsorption selectivity proposed in the Introduction.

3.3.3. FTIR results

FTIR spectroscopy was employed to characterize the mineral surfaces before and after STAC treatment, as illustrated in Fig. 9.

As demonstrated in Fig. 9 (a), in the infrared spectrum of brucite, the strong absorption peak at 3689.56 cm^{-1} is attributed to the O–H stretching vibration; the absorption peaks at 958.12 cm^{-1} and 609.91 cm^{-1} correspond to the Mg–OH lattice vibration and the Mg–OH out-of-plane bending vibration, respectively. In the spectrum of quartz (Fig. 9(b)), the strong absorption peak at 1079.52 cm^{-1} is attributed to the asymmetric Si–O–Si stretching vibration; the absorption peaks at 797.09 cm^{-1} and 694.18 cm^{-1} correspond to the symmetric Si–O–Si stretching vibration and the bending vibration, respectively; the absorption peak at 462.35 cm^{-1} in the low-frequency region can be attributed to the Si–O–Si bending vibration or the O–Si–O deformation vibration. The assignment of these characteristic peaks is generally consistent with the findings reported in Reference (Mao et al., 2024; Cheng et al., 2024), confirming the reliability of FTIR technology in identifying surface functional groups of brucite and quartz, and providing an important spectroscopic basis for subsequent analysis of the adsorption mechanism of STAC on mineral surfaces.

In the infrared spectrum of STAC, the characteristic absorption peaks at 2917.41 cm^{-1} and 2848.73 cm^{-1} are attributed to the symmetric stretching vibrations of the methylene ($-CH_2-$) and methyl ($-CH_3$) groups in the alkane chain. These are the most representative characteristic peaks of quaternary ammonium collector agents and serve as direct evidence for identifying the adsorption behavior of such

agents on mineral surfaces (Yu et al., 2025; Sun et al., 2026). After STAC treatment, new absorption peaks appeared in the infrared spectrum of quartz at 2917.87 cm^{-1} and 2849.13 cm^{-1}, which essentially match the vibrational characteristics of the alkyl chains in STAC, indicating that STAC has successfully adsorbed onto the quartz surface. In contrast, no new characteristic absorption peaks were observed in the IR spectrum of brucite after STAC treatment, indicating that only negligible adsorption of STAC occurs on the brucite surface.

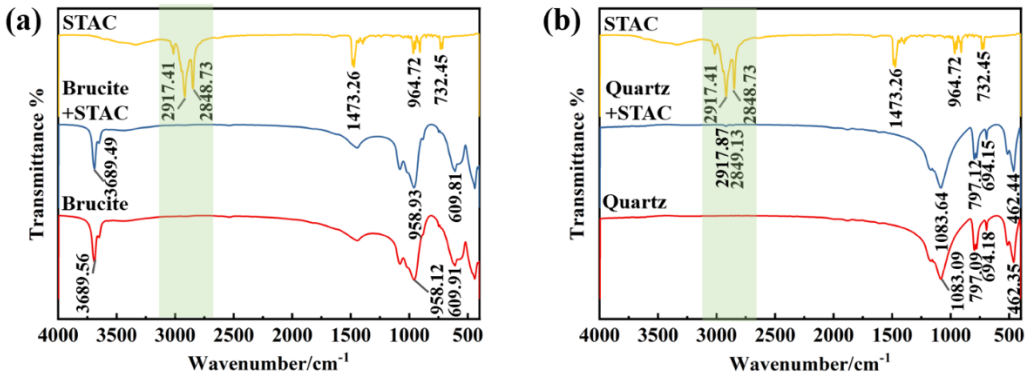

Fig. 9. FTIR spectra of brucite (a) and quartz (b) before and after STAC treatment.

3.3.4. XPS results

To gain a deeper understanding of the adsorption mechanism of STAC on mineral surfaces, XPS was used to analyze changes in the elemental composition, valence states, and surface composition of the mineral surfaces before and after STAC treatment under optimal flotation conditions (Xing et al., 2025; He et al., 2026). The results are shown in Fig. 10 and Fig. 11. Table 3 lists the binding energies and elemental concentrations of the two minerals before and after STAC treatment.

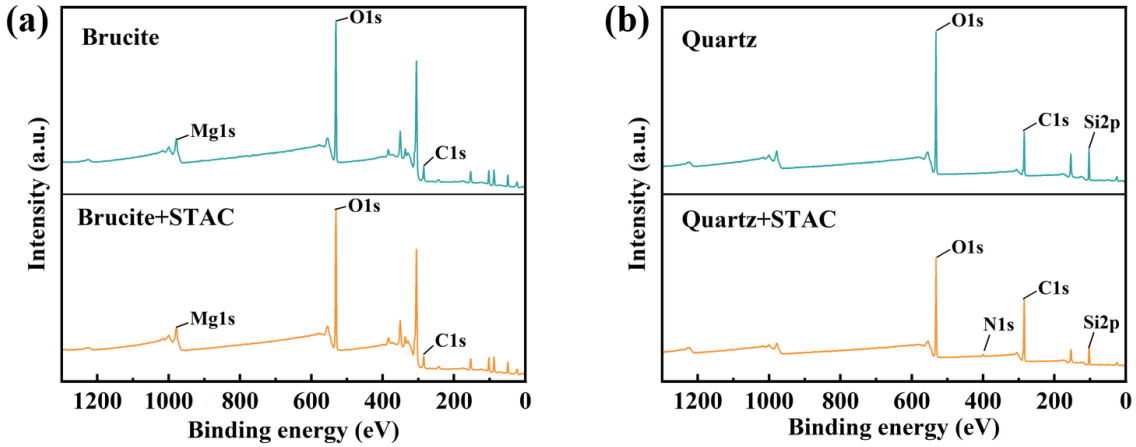

Fig. 10. XPS spectra of brucite (a) and quartz (b) before and after STAC treatment

As displayed in Fig. 10(a), the untreated brucite surface exhibits characteristic peaks corresponding to Mg 1s, O 1s, and C 1s. After STAC treatment, the surface chemical composition remained essentially unchanged, with no new characteristic peaks observed. For quartz, as depicted in Fig. 10(b), the untreated surface displayed characteristic peaks of O 1s, C 1s, and Si 2p. Following STAC treatment, a distinct N1s peak appeared in the XPS spectrum, originating from the nitrogen in STAC $[(CH_3)_3N^+C_{18}H_{37}]Cl^-$. Together with the FTIR results and the significant increase in contact angle, this result confirms the selective adsorption of STAC on the quartz surface, whereas its adsorption on brucite is negligible.

Table 3 shows the changes in the elemental composition of the brucite and quartz surfaces before and after STAC treatment. After STAC treatment, the N1s content on the quartz surface increased to

3.11%, while the C1s content rose significantly from 29.12% to 55.87%. This change indicates significant adsorption of STAC on the quartz surface. At the same time, the decrease in O1s content is likely due to the surface being covered by organic molecules, thereby reducing the exposure of oxygen atoms. In contrast, the surface composition of brucite showed minimal changes after STAC treatment: the C1s concentration rose only slightly from 26.71% to 27.04%, no N1s signal was detected, and the O1s concentration remained essentially unchanged. These results further confirm that STAC selectively adsorbs onto the quartz surface, whereas only negligible adsorption occurs on the brucite surface.

Table 3. Binding energy and surface element composition of minerals with and without STAC treatment

Sample	Elemental content % (Binding energy /eV)				
	Mg1s	Si_2p	C1s	O1s	N1s
Brucite	12.98 (1303.19)	0	26.71 (284.40)	38.04 (531.02)	0
Brucite+STAC	10.93 (1303.26)	0	27.04 (284.80)	40.46 (531.12)	0
Quartz	0	23.87 (103.74)	29.12 (284.40)	47.41 (532.41)	0
Quartz+STAC	0	14.05 (103.81)	55.87 (284.40)	39.27 (532.09)	3.11 (400.17)

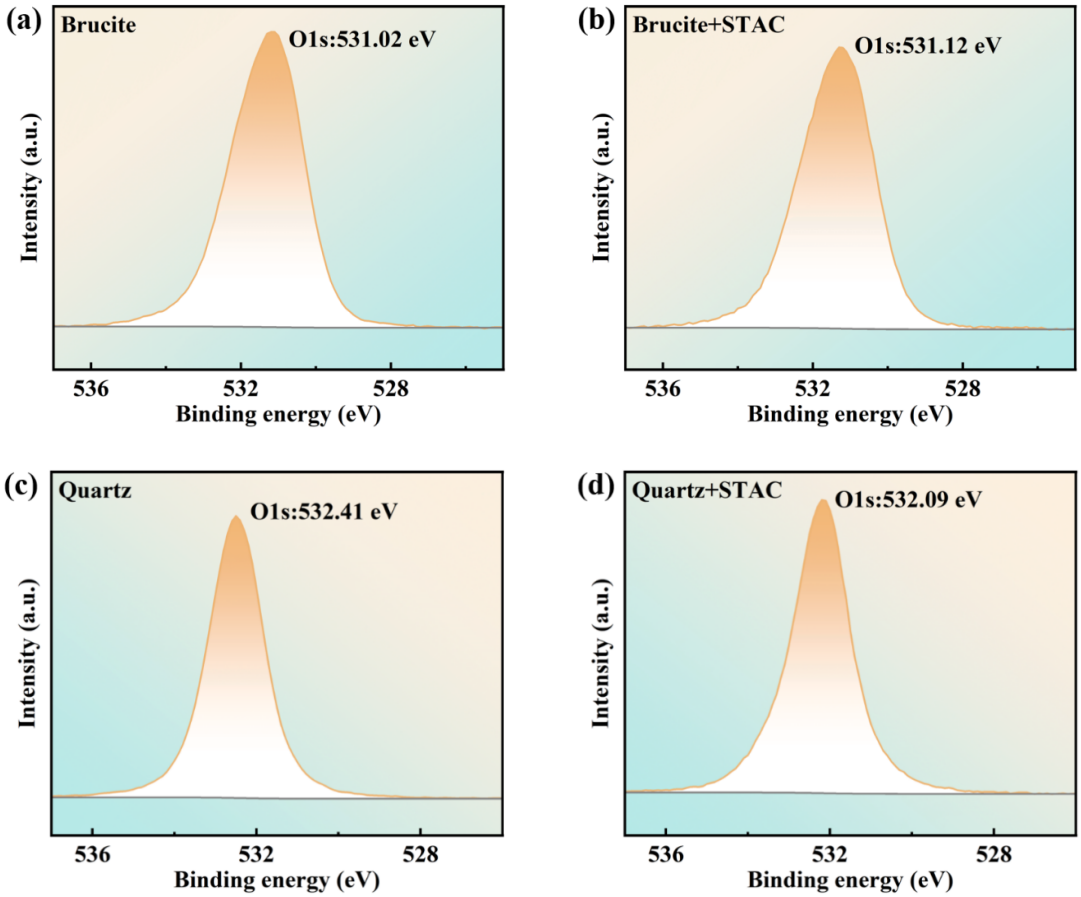

Fig. 11. Binding energies of oxygen atoms in brucite (a, b) and quartz (c, d) before and after STAC treatment

The O 1s binding energies of brucite and quartz are shown in Fig. 11. As indicated in Figs. 11(a) and (b), after STAC treatment, the O 1s binding energy of brucite increased only slightly from 531.02 eV to 531.12 eV, a change of just 0.10 eV. In contrast, as shown in Figs. 11(c) and (d), the O 1s binding energy of quartz decreased significantly from 532.41 eV to 532.09 eV, with a change of -0.32 eV. The change in

the O 1s binding energy of quartz is approximately 3.2 times that of brucite, indicating a strong interaction between the positively charged quaternary ammonium headgroup of STAC and oxygen sites on the quartz surface. Although weak non-classical C–H···O interactions cannot be completely excluded, the observed O 1s binding-energy shift is primarily attributed to electrostatic attraction. In contrast, the interaction between STAC and oxygen sites on the brucite surface is negligible, resulting in only weak adsorption. These findings are consistent with FTIR, contact-angle, zeta-potential and XPS analyses, collectively confirming the selective adsorption of STAC on quartz.

3.4 Modeling the separation of brucite and quartz

Based on experimental and mechanistic studies, Fig. 12 schematically illustrates the process by which STAC achieves the selective flotation separation of brucite and quartz through electrostatic adsorption.

As illustrated in Fig. 12, at pH 7.0, the surface of quartz (left, white sphere) carries a negative charge and adsorbs the positively charged STAC molecules via electrostatic attraction. The STAC molecules are oriented with their quaternary ammonium head groups toward the mineral surface and their hydrophobic alkyl tails extending outward, thereby forming a dense hydrophobic layer. This hydrophobic modification allows quartz to adhere effectively to air bubbles and rise into the froth phase, enabling its selective flotation recovery. In contrast, under identical pH conditions, the surface of brucite (right, black sphere) carries a positive charge. This results in strong electrostatic repulsion between the positively charged STAC molecules and the brucite surface, which inhibits significant reagent adsorption. Consequently, the brucite surface remains hydrophilic, which suppresses bubble attachment and allows brucite to remain in the cell as the sink product. In summary, STAC selectively adsorbs onto the negatively charged quartz surface via electrostatic interactions, rendering it hydrophobic and floatable. Conversely, electrostatic repulsion prevents its adsorption on the positively charged brucite surface, allowing brucite to retain its hydrophilicity and report to the sink product as the final concentrate. This charge-based selective adsorption is the fundamental mechanism underlying the efficient flotation separation of brucite and quartz achieved by STAC.

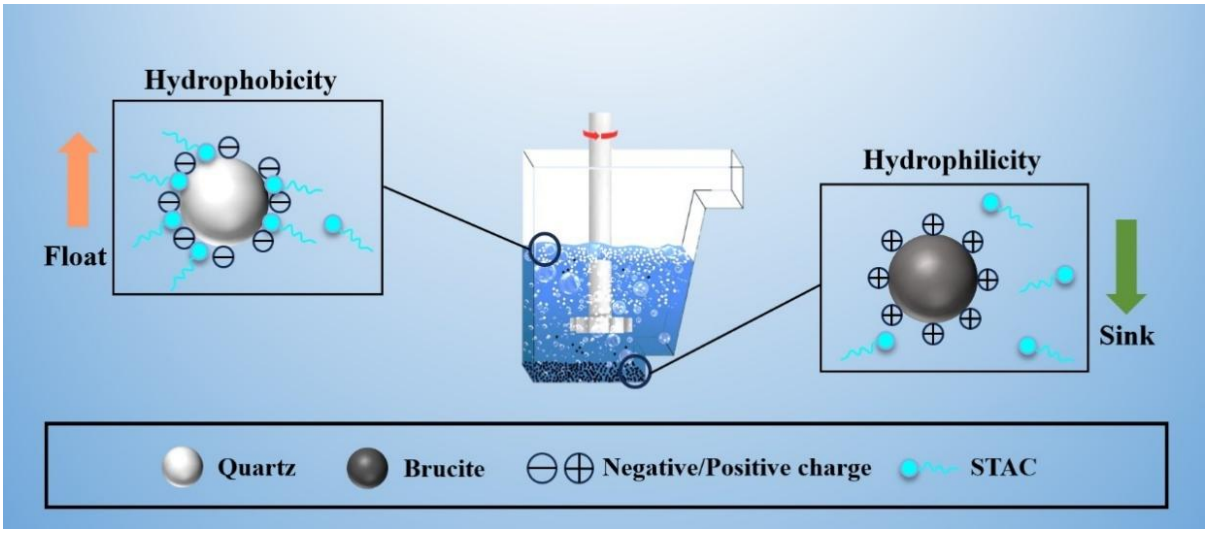

Fig.12. Schematic diagram of the mechanism of selective flotation separation of brucite and quartz by STAC

4. Conclusions

This study systematically investigated the flotation separation of brucite and quartz using STAC as a collector. Through integrated flotation performance tests, interfacial property characterization, and microscopic mechanism analysis, the selective separation behavior of STAC toward the two minerals and its underlying mechanism were elucidated. The main conclusions are as follows:

1. Flotation experiment results demonstrate that under optimal conditions (STAC concentration of 30 mg/L, pH 7.0, and agitation speed of 2000 rpm), quartz readily attaches to bubbles and floats, whereas brucite remains hydrophilic and sinks, achieving highly efficient selective separation of the two minerals.

2. Zeta potential and contact angle measurements confirmed that STAC selectively modifies the surface properties of the minerals. After STAC treatment, the changes in the contact angle and zeta potential of quartz were 7.82 and 57.1 times those of brucite, respectively, indicating that STAC selectively adsorbs onto the quartz surface while exhibiting negligible interaction with brucite.
3. Mechanistic insights from FTIR and XPS analyses reveal that the positively charged quaternary ammonium head of STAC preferentially binds to oxygen atoms on the quartz surface. The O 1s binding energy shift of quartz was 3.2 times that of brucite, clarifying the selective adsorption site and interaction strength. Electrostatic adsorption is identified as the core mechanism governing this selective separation.

Acknowledgments

This research received no specific grant from any funding agency in the public, commercial, or not-for-profit sectors.

References

AO, Y., HAN, C., SHEN, Y., MA, R., ZHAO, S., ZHAO, Q., CUI, B., 2026. *Investigation of surfactant effects on foam properties in quartz flotation with dodecylamine*. Colloids and Surfaces A: Physicochemical and Engineering Aspects, 737-1, 139749.

BAN, X., YAO, J., YIN, W., YIN, C., SUN, W., DU, W., ZHANG, T., WANG, Y., 2025. *Application of dodecylbenzenesulfonate isopropanolamine as an environmentally friendly collector in direct flotation separation of magnesite from quartz*. Minerals Engineering, 229, 109408.

CHENG, G., MA, Y., LÓPEZ-VALDIVIESO, A., YIN, W., 2024. *Selective depression of phenoxyacetyl chloride on magnesite: Implications for effective flotation separation of magnesite from dolomite*. Minerals Engineering, 218, 109017.

FU, Y., WANG, H., LIU, L., YAO, Q., YANG, X., HU, Z., YUAN, Q., YAO, J., LIU, J., 2023. *Regulation role of calcium lignosulfonate on the entrainment behavior of serpentine during brucite recycling: A new perspective*. Powder Technology, 428, 118764.

GONG, X., YAO, J., YANG, B., YIN, W., GUO, J., SONG, N., WANG, Y., SUN, H., 2023. *Activation-inhibition mechanism of diammonium hydrogen phosphate in flotation separation of brucite and calcite*. Journal of Environmental Chemical Engineering, 11-3, 110184.

GONG, X., YAO, J., YANG, B., YIN, W., WANG, Y., FU, Y., 2024. *Flotation separation of brucite and calcite in dodecylamine system enhanced by regulator potassium dihydrogen phosphate*. Transactions of Nonferrous Metals Society of China, 34-8, 2658-2670.

HE, J., YUAN, S., GAO, P., WANG, X., TIAN, P., TANG, Z., 2026. *Probing the interfacial adsorption mechanism of an ammonium salt of N-nitroso-N-phenylhydroxylamine in bastnaesite flotation by FT-IR, XPS and DFT*. Applied Surface Science, 719, 165103.

HU, T., DENG, J., SUN, R., XING, D., WANG, T., YIN, H., HU, Y., 2026. *Evaluation of CMCS as an environmentally friendly depressant for flotation separation of magnesite and quartz: Experiments and DFT calculations*. Applied Surface Science, 724, 165717.

KRUSZELNICKI, M., POLOWCZYK, I., KOWALCZUK, P., 2024. *Insight into the influence of surface wettability on flotation properties of solid particles – Critical contact angle in flotation*. Powder Technology, 431, 119056.

LI, H., WEI, G., DENG, S., TAN, B., LI, X., 2025. *Octadecyl dimethyl benzyl ammonium chloride as a novel efficient inhibitor for cold rolled steel in sulfuric acid*. Colloids and Surfaces A: Physicochemical and Engineering Aspects, 715, 136680.

LI, S., DENG, S., DU, P., DING, L., TAN, Y., WEI, R., LI, X., 2026. *A comparative study of octadecyl dimethyl betaine and octadecyl trimethyl ammonium chloride as corrosion inhibitors for steel in dichloroacetic acid*. Journal of Molecular Structure, 1351-2, 144335.

LIU, J., YIN, W., WANG, Y., HAN, H., YANG, B., YIN, X., YAO, J., ZHANG, Z., SUN, H., 2025. *Green 2-hydroxybenzoic acid-ASDA-Na_4 synergistic system induces morphology-controlled anhydrous $MgCO_3$ synthesis via magnesium leaching and carbonation from brucite solid waste*. Chemical Engineering Journal, 520, 166026.

LIU, S., ZHANG, W., REN, Q., TU, R., QIU, F., GAO, Z., XU, S., SUN, W., TIAN, M., 2024. *Innovating an amphoteric collector derived from dodecylamine molecular structure: Facilitating the selective flotation separation of apatite from quartz and dolomite*. Minerals Engineering, 215, 108819.

LIU, W., MAO, Y., WANG, B., ZHAO, Q., ZHAO, S., GAO, S., LIU, W., SHEN, Y., 2025. *Novel insights into enhancing the flotation separation of low-grade magnesite ore: Effect behavior and mechanism of adding diethanolamine.* Materials Today Communications, 48, 113407.

MA, X., NGUYEN, N., NGUYEN, A., MILLER, J., 2023. *An investigation of mineral floatability versus mineral surface exposure and hydrophobicity by high-resolution X-ray microcomputed tomography, film flotation, contact angles, and modeling*. Minerals Engineering, 200, 108139.

MAO, Y., LIU, W., LIU, W., SHEN, Y., ZHAO, Q., 2024. *Exploring the behavior of an alcoholic amine grinding aid in grinding-flotation system: Separation of quartz from magnesite*. Journal of Molecular Liquids, 411, 125783.

SUN, H., GAO, G., WANG, Y., 2024. *Mechanism of action of the novel reagent dodecyl trimethyl ammonium chloride on magnesite and quartz surfaces.* Journal of Molecular Liquids, 414, 123184.

SUN, H., GAO, G., WANG, Y., SUN, Y., GUO, Z., 2025. *Selective depression of dolomite in magnesite flotation using a novel chelating depressant MGDA: Adsorption mechanism and DFT calculations*. Colloids and Surfaces A: Physicochemical and Engineering Aspects, 727-2, 138300.

SUN, H., GUO, Z., WANG, Y., ZHANG, F., CAO, S., YIN, W., YAO, J., 2026. *Multifaceted study on selective activation of brucite and quartz by cationic collector EQ-90: Flotation experiments, surface modulation, induction time.* Applied Surface Science, 716, 164692.

SUN, Y., YAO, J., YIN, W., SUN, H., YANG, S., 2025. *Selective flotation of quartz from brucite with methylammonium imidazoline sulfate oleate: Mechanisms and surface chemistry insights*. Separation and Purification Technology, 379, 134904.

SUN, Y., YAO, J., YIN, W., SUN, H., YANG, S., CHEN, Y., 2026. *Unveiling ODDAC's selective adsorption mechanism for magnesite-quartz reverse flotation via TOF-SIMS microscopic site mapping*. Journal of Environmental Chemical Engineering, 14-1, 120948.

SUN, Y., YAO, J., YIN, W., SUN, H., YANG, S., 2025. *Esterquat EQ-90 as a green novel collector for effective desilication in magnesite flotation: Adsorption mechanisms and selectivity*. Minerals Engineering, 232, 109543.

XING, D., HU, T., WANG, T., DENG, J., DIAO, Y., CHENG, T., HAN, J., YANG, Y., 2025. *Non-toxic and biodegradable depressant Gum Arabic for flotation separation of calcite and magnesite: Experiments and MD simulations.* Advanced Powder Technology, 36-9, 104992.

YAO, J., BAN, X., XIE, Y., YIN, W., WANG, Y., XUE, F., 2024. *Research advancement of efficient flotation separation technologies for magnesium-containing minerals*. Green and Smart Mining Engineering, 1(2), 140-156.

YAO, J., SUN, Y., YIN, W., SUN, H., YANG, S., 2025. *Study on the effects of a novel imidazoline siliconophilic collector in the desilication process of magnesite: Separation experiments, adsorption mechanisms, and separation model*. Separation and Purification Technology, 353, 128461.

YIN, W., FAN, Y., XIE, Y., 2025. *Application of nano-collector in mineral flotation: A review*. Powder Technology, 444, 121430.

YU, J., YAO, J., YIN, W., GONG, X., YIN, X., ZHAO, X., 2025. *Study on the adsorption mechanism of green and efficient flotation reagents in the reverse flotation separation of limonite and quartz*. Colloids and Surfaces A: Physicochemical and Engineering Aspects, 726-1, 137849.

ZHANG, F., LI, X., DENG, S., TANG, M., DU, G., 2021. *Amphoteric surfactant of octadecyl dimethyl betaine as an efficient corrosion inhibitor for cold rolled steel in phosphoric acid solution*. Journal of Materials Research and Technology, 15, 7050-7069.

ZHANG, W., WANG, Z., TIAN, H., LIU, J., GUO, Z., LIU, P., TIAN, M., XIE, L., 2024. *Experimental evidence supporting distinct adsorption configurations of N,N-bis(2-hydroxy-3-chloropropyl) dodecylamine and dodecylamine on apatite surfaces: Quartz crystal microbalance and atomic force microscopy studies*. Surfaces and Interfaces, 51, 104681.

ZHAO, Q., YANG, H., TONG, L., JIN, R., MA, P., 2022. *Understanding the effect of grinding media on the adsorption mechanism of cyanide to chalcopyrite surface by ToF-SIMS, XPS, contact angle, zeta potential and flotation.* Colloids and Surfaces A: Physicochemical and Engineering Aspects, 644, 128799.

ZHU, Y., ZHANG, Y., WANG, J., JIA, S., MA, Y., LI, G., ZHENG, Q., 2026. *Controlled synthesis of $Mg(OH)_2$ with tailored crystal morphologies from brucite via hydration: Morphological evolution mechanism and hydration kinetics.* Journal of Crystal Growth, 679, 128501.